



Supercontinuum generation based on suspended core fiber infiltrated with butanol

Thuy Nguyen Thi¹ · Lanh Chu Van²

Received: 13 December 2022 / Accepted: 13 July 2023
© The Author(s), under exclusive licence to The Optical Society of India 2023

Abstract Supercontinuum generation in silica-suspended core fibers infiltrated with butanol has been analyzed numerically. The spectra spanning from 806.19 to 1520.56 nm is generated in #F₁ fiber ($D=65.887\ \mu\text{m}$) with an all-normal dispersion regime pumped by a 13.33 kW peak power of laser source at 1.3 μm . With anomalous dispersion of two closely lying zero dispersion wavelengths, #F₂ fiber ($D=67.494\ \mu\text{m}$) creates supercontinuum based on self-phased modulation, phasematched four-wave mixing, and no soliton fission as in the initial photonic crystal fibers pumped in the anomalous dispersion region. A broad spectrum of 629.12 nm is obtained when this fiber is excited at the same wavelength as the #F₁ fiber with a peak power of 12.5 kW. Butanol infiltration into three air holes significantly improved the dispersion properties of the fibers, contributing to supercontinuum generation advantage. The smooth, noise-free supercontinuum spectrum can be compressed into ultra-short pulses.

Keywords Suspended core fibers · Butanol · Supercontinuum generation · Two zero dispersion wavelengths

Introduction

Supercontinuum (SC) generation is a process in which a broadband light is generated by expanding narrow band

optical pulse in the frequency domain. This is the result of an optical short pulse interaction with a nonlinear material involving different nonlinear optical effects such as self phase modulation, cross phase modulation, Raman scattering, four wave mixing etc., [1]. Recently, SC generation has been a subject of great interest in nonlinear optics and has attracted the attention of scientists around the world due to outstanding features and properties such as: high coherence, large bandwidth, brightness, high power output, and potential compactness. The appearance of photonic crystal fibers with many special properties depending on lattice structures has replaced conventional optical fibers in applications including SC generation. Supercontinuum laser sources using photonic crystal fibers have an important role in applications for chemical and biomedical sensing, gas sensor, military applications, and materials processing [2–11].

The photonic crystal fibers are designed with a variety of geometrical cores including square core, circular core, regular hexagonal core, octagonal core, suspended core, etc., to select the optimal structure for different applications. Among them, suspended core fiber (SCF) is an ideal candidate for further enhancing nonlinear properties and improving dispersion engineering. Along with the significant applications in nonlinear optics, SCF has become a hot topic of intense research in recent decades. “Suspended-core fiber” was first suggested by Monro et al. [12], then SCFs based on lead silicate glass and tellurite with highly nonlinear and anomalously dispersive were reported in [13–15]. In the experiment, a simple SCF fabrication method was described, this technique consists of mechanical drilling of the holes of the preform, and the shape of the holes approximates that of an air-suspended rod with three fine struts supporting the core [16]. Since then, SCF has been a relatively new class of fibers as a subclass of microstructured. In these

✉ Lanh Chu Van
chuvanlanh@vinhuni.edu.vn

¹ University of Education, Hue University, 34 Le Loi, Hue City, Vietnam

² Department of Physics, Vinh University, 182 Le Duan, Vinh City, Vietnam

fibers, a tiny core is suspended by very thin struts, usually three submicron ultrathin glass bridges, connected to the outer cladding [17, 18]. This keeps the core isolated from the outside environment resulting in strong confinement of light. Because of liquid or gas space between thin glass bridges, the interaction between guided light and matter through evanescent fields offers promising opportunities for sensing applications including chemical sensors, biomedical sensors, and high sensitivity label-free measurements of the biological sample [18–23], as well as the application for explosive detection and DNA identification [8–10].

The shape, size, number, and thickness of the glass bridges and the diameter of the core of SCF have been studied both theoretically and experimentally to improve birefringence or nonlinear properties leading to enhanced SC generation efficiency [24–33]. However, it is difficult to broaden the SC spectrum in the mid-infrared region based on silica-based photonic crystal fibers because pure silica has a high phonon energy, about 1100 cm^{-1} [34]. Compared with solids, liquids have a higher nonlinear refractive index, which makes it easier to observe nonlinear phenomena, such as optical solitons, so fibers SCFs infiltrating liquids are an excellent alternative. By filling the air holes in silica SCF with various liquids, the characteristic dispersion curvature, the flatness, normal and anomalous properties of chromatic dispersion could further be altered dramatically. These advantages are quite suitable for the SC generation to further broaden the spectrum based on two main mechanisms: First, self-phase modulation (SPM), followed by optical wave breaking (OWB) are the two main effects that cause a broad, flat, and highly coherent when using PCFs with an all-normal dispersion regime. Second, a broader SC spectrum can be generated via PCFs with anomalous dispersion with one and two ZDWs where the soliton dynamics include soliton fission (SF), soliton frequency self-shift (SSFS), and dispersed wave blue shifts (DWs) are responsible for the spectrum expansion.

The replacement of air with water can improve typical SCF dispersion characteristics into all-normal near-zero

flat dispersion characteristics, valuable in the process of supercontinuum generation, which extends the spectrum to about 700 nm [32]. In SCF infiltrated with water [33], the all-normal dispersion supercontinuum was generated with spectral coverage from 435 to 1330 nm using a laser source with a peak power of 150 kW and 800 nm central wavelength. Through both theoretical and experimental birefringence analyses, the sensitivity of the temperature sensor is proved to be strongly affected when the air holes of the SCF are filled with ethanol [35]. The advantage of carbon tetrachloride permeation in enhancing the nonlinearity of SCF is demonstrated in [36]. An ultrabroad supercontinuum of width $\approx 722\text{ nm}$ was simulated by passing a pulse of 5 kW peak power. In addition, other fluids such as heavy water, chloroform, carbon tetrachloride, toluene, nitrobenzene, carbon disulfide, tetrachloroethylene, ethanol, etc. are also selected by the researchers to improve the nonlinear properties of photonic crystal fibers and extend the spectrum of supercontinuum generation [37–49]. However, publications focused mostly on photonic crystal fibers with hexagonal, circular or square lattices not suspended core fibers. Some research results on SC generation through silica-based SCF filled with other liquids are shown in Table 1.

To our knowledge, up to now, there has been no work to study nonlinear properties and supercontinuum generation of silica SCF with core infiltrated with butanol. We present for the first time a numerical study of the dependence of the total diameter of air hole structure D on the dispersion characteristics of SCFs. Through detailed analysis of the nonlinear properties of butanol fibers, we propose two structures #F₁ and #F₂, with suitable flat dispersion and high nonlinear coefficient of $13.437\text{ W}^{-1}\cdot\text{km}^{-1}$ and $13.058\text{ W}^{-1}\cdot\text{km}^{-1}$ at $1.3\text{ }\mu\text{m}$ pump wavelength for using in supercontinuum generation. By pumping 10 cm long samples of these fibers, we observed the infrared supercontinuum generation expanded from 806.19 to 1520.56 nm with the peak power of 13.33 kW for #F₁ fiber and 879.96 nm to 1509.08 nm wavelengths with the peak power of only 10 kW for #F₂ fiber.

Table 1 Overview SC generation in several liquids-infiltrated silica-based SCFs

Structures	Liquids	Fiber length (cm)	Pump wavelength (μm)	Dispersion regime	SC range (nm)	Input peak power (kW)	References
SCF #F ₃	Water	10	1.064	All-normal	About 700	20	[32]
SCF #F ₅		100	1.064	Anomalous	About 800	0.33	
SCF	Water	12	0.8	Anomalous	895	150	[33]
SCF	Air	12	0.8	All-normal	800	150	
SCF	Carbon tetrachloride	5	1.55	Anomalous	722	5.0	[36]
SCF (SF = 1.44)	Carbon disulfide	100	1.55	Anomalous	672	100	[49]

Numerical modeling of the SCF

For simulation, we used silica (SiO₂) based SCF with three air holes infiltrated with butanol (C₄H₉OH); the light is propagated in the defect of the fiber structure. Our SCFs are designed using Lumerical Mode Solutions software (LMS) with the full-vector finite-difference eigenmode (FDE) method. To increase the numerical accuracy of the simulations, FDE solves Maxwell’s equations by dividing the fiber’s cross-section into smaller rectangular sections of hundreds of thousand parts. The boundary condition is the perfectly matched classes positioned outside the outermost ring of holes to reduce the loss as small as possible. We assume the loss of butanol is negligible during the simulation of the optical properties of SCFs. The simulation of the SCFs is carried out as follows: first, butanol and pure silica are put into the LMS data system by entering the refractive index according to the Sellmeier equation [49] and the Cauchy equation [50] and the attenuation data of butanol are also fully declared. Next, the SiO₂ base material is created, and suspended core-structures are designed by introducing SEM images of real fibers into the system. Finally, the air in the fiber defect is completely replaced with butanol, and the input parameters are thoroughly tested before simulating the optical properties of the SCFs. In the experiment, the liquid-infiltrated SCF was also fabricated using the standard stack-and-draw method. The liquid is filled into the defective part of the fiber by integrating a microfluidic pump system using a thermal fusion splicer or laser writing technique. The infiltration of a 60 cm-long fiber sample takes about 1 min [33].

The schematic cross-section geometrical structure of the SCF is shown in Fig. 1. To increase modal nonlinearity and optimize SCF structure for dispersion, SCFs

were designed with different lattice parameters such as: radius of holes R_{hole} , radius of the core r_c , thickness of glass bridge t_c , and a total diameter of air-hole structure D . D is varied from 32.140 μm to 72.314 μm. Figure 1b shows that the light is strongly confined to the core of SCF with $D = 65.887$ μm.

The dependence of refractive index characteristics on wavelength for butanol modeled following Cauchy’s equation [50] and given by the formula:

$$n^2(\lambda) = A_0 + A_1\lambda^2 + \frac{A_2}{\lambda^2} + \frac{A_3}{\lambda^4} + \frac{A_4}{\lambda^6} \tag{1}$$

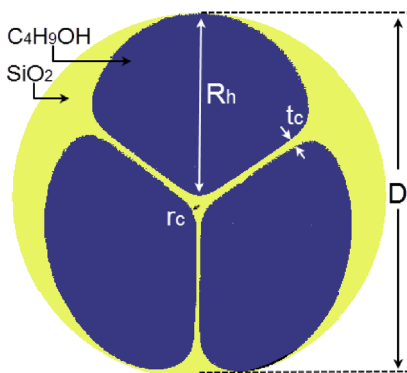
where $A_0 = 1.913001067$; $A_1 = -0.00152344 \mu\text{m}^{-2}$, $A_2 = 0.01303537 \mu\text{m}^2$, $A_3 = -0.00198394 \mu\text{m}^4$, $A_4 = 0.000275162 \mu\text{m}^6$ and λ is the operating wavelength in micrometers.

With the fused silica, the refractive index can be obtained using Sellmeier’s equation [50], where λ is the wavelength in micrometers.

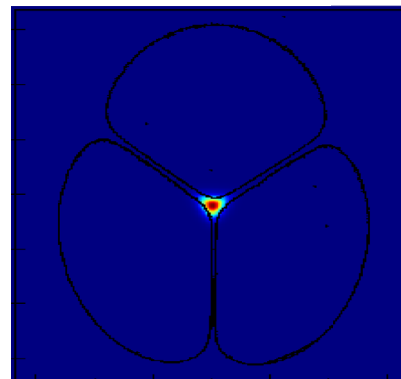
$$n_{\text{Fused silica}}^2(\lambda) = B_0 + \frac{B_1\lambda^2}{\lambda^2 - C_1} + \frac{B_2\lambda^2}{\lambda^2 - C_2} + \frac{B_3\lambda^2}{\lambda^2 - C_3} \tag{2}$$

with coefficients: $B_0 = 1$; $B_1 = 0.6694226$, $B_2 = 0.4345839$, $B_3 = 0.8716947$, $C_1 = 4.4801 \times 10^{-3} \mu\text{m}^2$, $C_2 = 1.3285 \times 10^{-2} \mu\text{m}^2$, $C_3 = 95.341482 \mu\text{m}^2$.

Butanol is a solvent with a high nonlinear refractive index. It is less toxic and quite safe for humans as well as the environment, and very convenient in the fabrication and the use of PCFs for practical application. The real parts of the refractive index of butanol and fused silica [50] are shown in Fig. 2. Reliable data are available only for the wavelength range of 0.6–2.0 μm, so we limited the simulation to this range.



a The geometrical structures of PCF with suspended core (SCF)



b The geometrical structures of SCF and light is confined in the core of SCF with $D = 65.887$ μm

Fig.1 **a** The geometrical structures of PCF with suspended core (SCF) **b** The geometrical structures of SCF and light is confined in the core of SCF with $D = 65.887$ μm

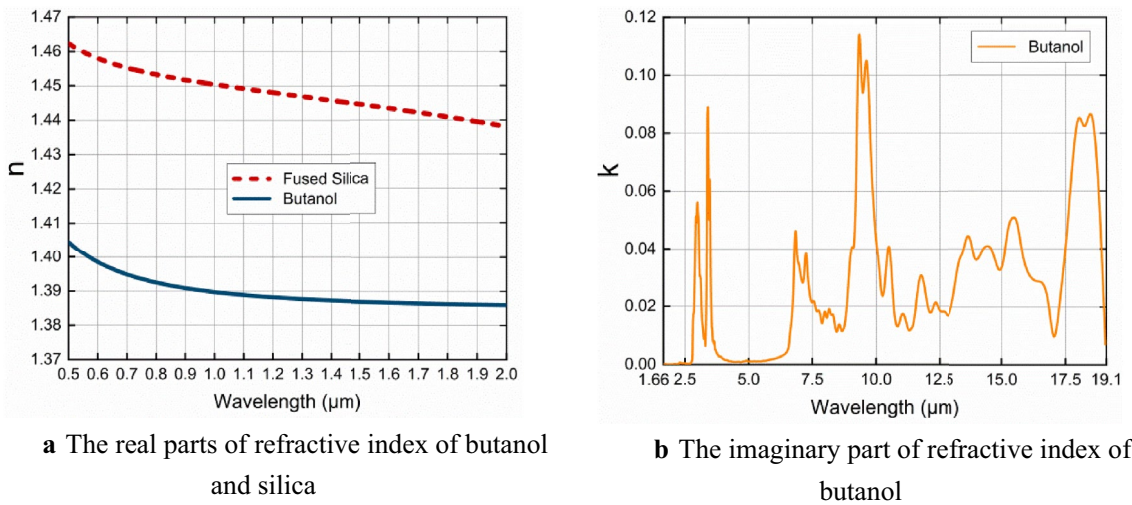


Fig. 2 a The real parts of refractive index of butanol and silica. b The imaginary part of refractive index of butanol

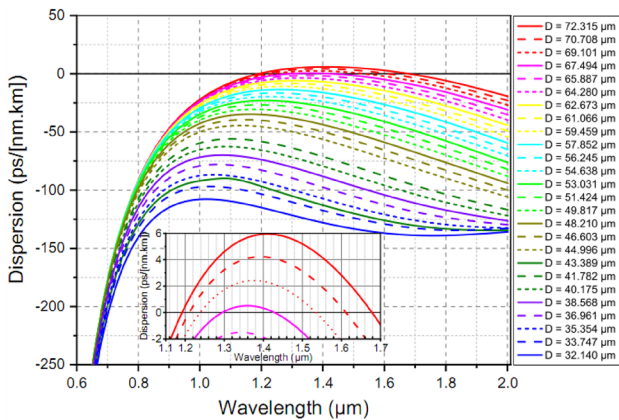


Fig. 3 The dispersion characteristics of PCF with various values of total diameter of air-hole structure

Dispersion properties of the SCF

The dispersion coefficient, including both waveguide and materials dispersion, is proportional to the second derivative of the effective index of guided mode with respect to wavelength and is given by formula [1].

$$D = -\frac{\lambda}{c} \frac{d^2 Re[n_{eff}]}{d\lambda^2} \quad (3)$$

where $Re[n_{eff}]$ is the real part of n_{eff} which is effective index of a guided mode calculated by means finite difference method and c is the velocity of light in vacuum. The dispersion characteristics with various values of the total diameter of the air-hole structure are presented in Fig. 3. The dispersions curve shape of fibers with various wavelengths does not change much with a varying total diameter of the

air-hole structure, and the values of dispersion increase with the increase in total diameter of the air-hole structure. On the other hand, increasing the total diameter of the air-hole structure leads to a flattening of the dispersion in the range with $\lambda > 0.9 \mu\text{m}$. SCFs with butanol infiltration exhibit both the all-normal and anomalous dispersion with a larger shift of zero dispersion wavelengths (ZDWs) towards the longer wavelength region. The butanol infiltration strongly affects the dispersion curve. Anomalous dispersion properties are found in large core fibers with a total diameter of air-hole structure greater than 65.887 μm, with two ZDWs. The zero-dispersion wavelengths (ZDW_1) are located around 1.15–1.30 μm, and the other one (ZDW_2) is from 1.40 to 1.65 μm range. Shifting the ZDW toward long wavelengths is extremely important if we consider the use of the SCFs for soliton-driven supercontinuum with low-cost short-pulse microchip lasers [33]. In the rest cases, the dispersion is completely located in the all-normal dispersion region; increasing the total diameter of the air-hole structure makes dispersion more and more flat and close to the zero dispersion line. Therefore, we can conclude that the flatness of the dispersion curve is controlled more effectively by the total diameter of the air-hole structure. In works [40–47], both all-normal and anomalous dispersion were also observed in photonic crystal fibers with different liquids infiltration. Variations in the lattice constant and the filling factor of structures affected the flatness of dispersion curves; one or two ZDWs were also found in these photonic crystal fibers. However, these results based on photonic crystal fibers with regular hexagonal not suspended core fibers.

Dispersion plays a very vital role in SC generation. The flatness, indication of the dispersion characteristic, and the compatibility of ZDW with the pump wavelength are significant factors, because they not only affect the SC

Table 2 The structure parameters of proposed PCFs

#	r_c (μm)	R_{hole} (μm)	t_c (μm)	D (μm)	Pump wavelength (μm)	A_{eff} (μm^2)	γ ($\text{W}^{-1} \cdot \text{km}^{-1}$)	D (ps/[nm.km])
#F ₁	1.681	31.2215	0.5125	65.887	1.3	10.788	13.437	-1.565
#F ₂	1.722	31.983	0.525	67.494	1.3	11.101	13.058	0.247

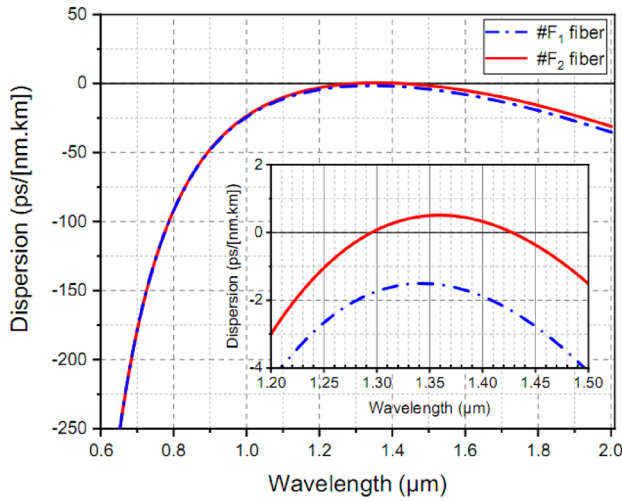


Fig. 4 Dispersion characteristics of #F₁ and #F₂ fiber

generation’s efficiency but also decide the expansion of the SC spectrum. On the basis of preliminary simulation, we proposed two optimal SCFs to analyze the SC generation because of their flat near-zero dispersion, namely #F₁ and #F₂. The geometrical parameters of the fibers are introduced in Table 2. The first fiber (#F₁) with $D = 65.887 \mu\text{m}$, exhibits the flattest all-normal dispersion characteristic in the whole analyzed wavelength range, is the blue curve in Fig. 4. The achieved SC spectrum would be the broadest by choosing the pump wavelength near the local maximum of the dispersion curve. Thus, this fiber is designed to use broad all-normal dispersion SC generation with the pump wavelength of $1.3 \mu\text{m}$, the dispersion is $-1.565 \text{ ps}/(\text{nm km})$. For fiber #F₂, ($D = 67.494 \mu\text{m}$), two ZDWs are observed at $1.2887 \mu\text{m}$ (ZDW_1) and $1.439 \mu\text{m}$ (ZDW_2), the dispersion at $1.3 \mu\text{m}$ is equal to $0.247 \text{ ps}/(\text{nm km})$. It is expected to generate the broad soliton-induced SC due to the very small value of dispersion at the pump wavelength. The value of all-normal dispersion of #F₁ fiber is 1.5–5 times smaller than that of photonic crystal fibers infiltrated with nitrobenzene [43], tetrachlorethylene [45], toluene [48]. This value of #F₂ fiber has anomalous dispersion is 13–136 times smaller than that of photonic crystal fibers infiltrated nitrobenzene [43] and tetrachlorethylene [45].

Figure 5 shows the dependence of the effective mode area on wavelength, the effective mode area of the proposed SCFs

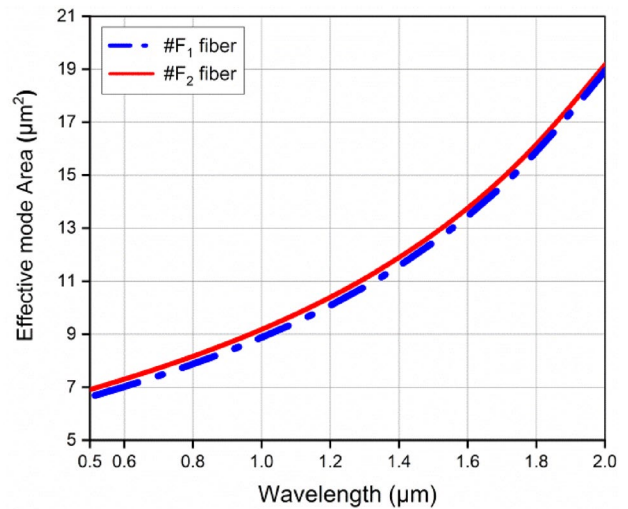


Fig. 5 Effective mode of the proposed SCFs

increases with the wavelength. It is a known fact that with the increase in wavelength, the modes get leaked through the holes and among them since the light is no longer confined strongly inside the core. With the large total diameter of air-hole structure, #F₂ fiber has a larger effective mode area than #F₁ fiber. The effective mode area for the fundamental mode of fiber #F₁ is $10.788 \mu\text{m}^2$ for a pump wavelength of $1.3 \mu\text{m}$, while that of #F₂ fiber is $11.101 \mu\text{m}^2$ at the same pump wavelength.

The nonlinearity of fiber is inversely proportional to the effective mode area. It can be determined by equation $\gamma = \omega_0 n_2 / c A_{\text{eff}}$, where n_2 is the nonlinear refractive index coefficient of silica, c is the velocity of light, and ω_0 is the central frequency of the pulse. The nonlinear coefficient of the proposed SCFs are presented in Fig. 6. The increase of effective mode area leads to a decrease of nonlinear coefficient of the fibers, this reduction is almost linearly with wavelength. With the filling of the air holes with butanol, the proposed PCFs have large nonlinear coefficients. The nonlinear coefficients of the two fibers are equal to $13.437 \text{ W}^{-1} \cdot \text{km}^{-1}$ and $13.058 \text{ W}^{-1} \cdot \text{km}^{-1}$ at a pump wavelength of $1.3 \mu\text{m}$. Table 2 displays dispersion values, effective mode regions, and nonlinearity coefficients at the pumping wavelength of the proposed fibers. Although the nonlinear coefficients at the pump wavelength of the two proposed fibers are not as high as the published optimized photonic crystal

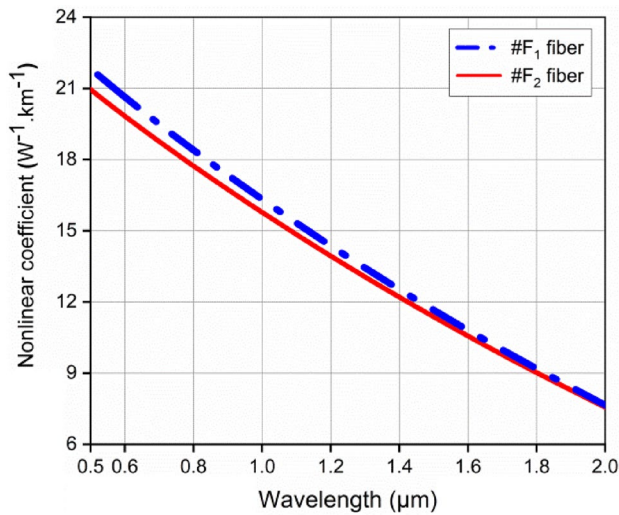


Fig. 6 Nonlinear coefficient of the proposed SCFs

fibers [36–38, 43–47], the effective mode area is lower than that in publications [43, 45, 47, 48] is a good condition to generate SC with lower peak power.

It should be noted that it is not easy to simultaneously optimize the characteristic quantities of the SCFs. The fibers with different characteristics will suit different specific applications.

Supercontinuum generation in proposed fiber

Due to the difference in dispersion properties, the two proposed fibers are expected to generate a broad SC spectrum with typical nonlinear effects. SPM followed by OWB are believed to be the main effects in SC spectral expansion when the input pulse is propagated in all-normal dispersion SCFs. Meanwhile, the soliton dynamics will govern the spectral expansion through SCFs with anomalous dispersion. However, the results of SC generation for #F₂ fiber are not the same as for conventional mechanisms, which may be due to the influence of its dispersion with two ZDWs.

An ultrashort pulse of light, when travelling in SCF with butanol infiltration, will induce a varying refractive index of the medium leading to nonlinear effects in SC generation. The equation evaluating the pulses the propagation in optimized structured fibers is given by the generalized nonlinear Schrödinger equation (GNLSE), using the symmetry split-step Fourier transform method [51] given by the formula:

Table 3 The coefficient of high-order dispersion at the pump wavelength

Coefficients	#F ₁	#F ₂
β ₂ (ps ² /m)	7.09 × 10 ⁻⁹	3.53 × 10 ⁻⁹
β ₃ (ps ³ /m)	-7.23 × 10 ⁻¹¹	-6.06 × 10 ⁻¹¹
β ₄ (ps ⁴ /m)	6.27 × 10 ⁻¹³	6.16 × 10 ⁻¹³
β ₅ (ps ⁵ /m)	-4.55 × 10 ⁻¹⁵	-3.94 × 10 ⁻¹⁵
β ₆ (ps ⁶ /m)	5.67 × 10 ⁻¹⁷	2.24 × 10 ⁻¹⁷
β ₇ (ps ⁷ /m)	-1.89 × 10 ⁻¹⁹	-2.87 × 10 ⁻¹⁹
β ₈ (ps ⁸ /m)	-2.79 × 10 ⁻²⁰	2.75 × 10 ⁻²¹
β ₉ (ps ⁹ /m)	4.69 × 10 ⁻²²	7.72 × 10 ⁻²³
β ₁₀ (ps ¹⁰ /m)	1.69 × 10 ⁻²³	-5.62 × 10 ⁻²⁵
β ₁₁ (ps ¹¹ /m)	-7.2 × 10 ⁻²⁵	-6.50 × 10 ⁻²⁶

$$\begin{aligned} \partial_z \tilde{A} - i\tilde{\beta}(\omega)\tilde{A} - \frac{\tilde{\alpha}(\omega)}{2}\tilde{A} \\ = i\gamma \left(1 + \frac{\omega - \omega_0}{\omega_0} \right) \tilde{A} F \left[\int_{-\infty}^{\infty} R(T') |A|^2 (T - T') dT' \right] \end{aligned} \quad (4)$$

where $A(z, \omega)$ is Fourier transform of the amplitude of a pulse $A(z, T)$, and $R(T)$ is Raman response function. The left side of Eq. (4) presents the effects of the linear operations, i.e., attenuation and dispersion of the fiber. $\tilde{\alpha}$ and $\tilde{\beta}$ are attenuation and dispersion in the frequency domain, respectively. The right-hand side of the Eq. (4) describes the nonlinear effects which depend on the nonlinear optical response of butanol determined by the combination of the bound-electronic and nuclear contribution. In this section, we analyze the SC generation only for the fundamental mode because the obtained higher-order dispersion coefficients (Table 3) are pretty small.

The numerical results of all-normal SC generation in #F₁ fiber are shown in Fig. 7. The input pulse has a wavelength of 1.3 μm, and propagates in 10 cm of fiber length with a duration of 120 fs. Self-phase modulation (SPM), and dispersion wave generation are the main effects, responsible for spectral expansion in all-normal dispersion SC generation.

Figure 7a depicts the evolution of the SC spectrum on input pulse energy which was set up in the range 0.1–1.6 nJ, corresponding to a peak power of 0.833–13.33 kW. The spectral bandwidth increases with increasing peak power. With low input energy (0.1 nJ), the SC spectrum is typically symmetry and narrow, the spectral broadening dominated by modulation instability. As the input pulse energy increases, the #F₁ fiber provides a low-noise broadband SC generation due to the SPM and oscillating structure. The spectrum caused by SPM consists of many peaks and the outermost peaks on the long wavelength side have the strongest intensity. In the case of higher input pulse energies of 1.2 nJ with peak powers of 10 kW respectively, the central pulse is initially broadened by

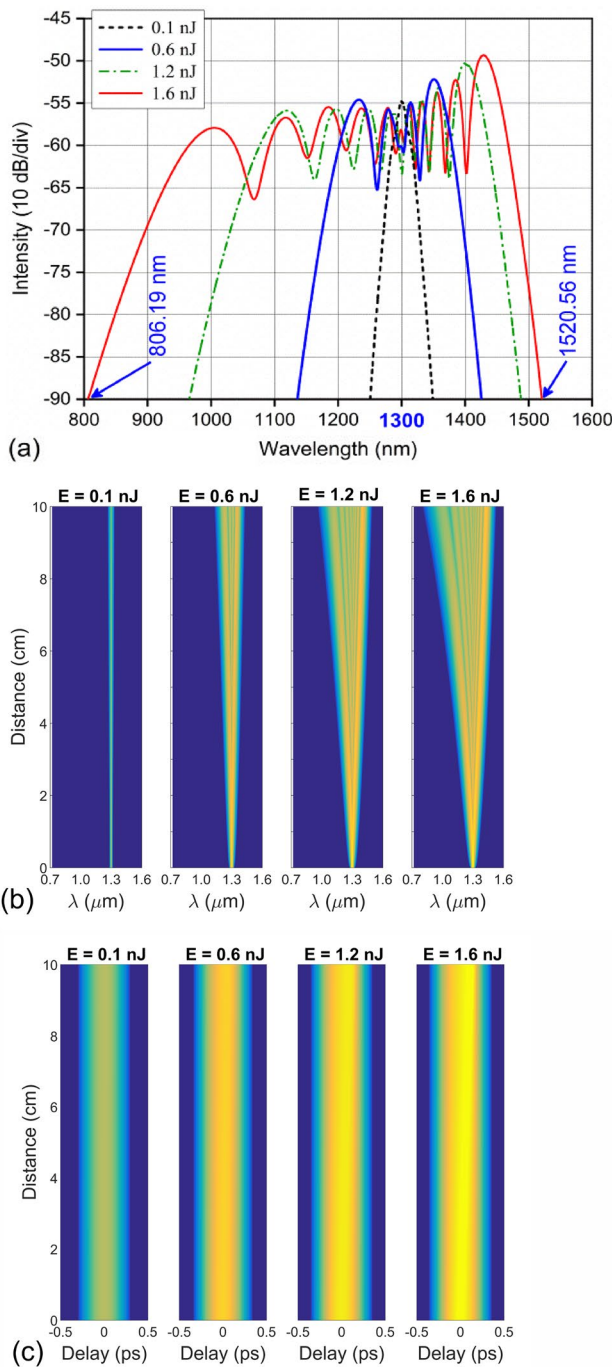


Fig. 7 For #F₁ fiber: **a** various input pulse energy in 10 cm length when pumped with pulses of 120 fs duration, 1.3 μm pump wavelength, **b** the temporal profile versus propagation length at various input pulse energies, and **c** the pulse evolution of the SC along with fiber

the SPM effect. Then, the interaction between the group velocity dispersion and the SPM causes the OWB to appear, which contributes to the spectral widening at the wings [52, 53]. The spectrum is no longer symmetric but extends towards the blue edge. With the maximum peak power of 13.33 kW (input pulse

energy of 1.6 nJ), the spectral bandwidth covers from 806.19 to 1520.56 nm within 10 dB dynamic range. Along with the enhancement of SPM, the spectrum on the blue edge continues to be broad due to the OWB. However, the spectral expansion on the short wavelength side will be limited by the high dispersion slope [54] if the peak power of the input pulse continues to increase. Furthermore, the large effective mode area and the high confinement loss in the long wavelength range also contribute to the inhibition of pulse expansion on the red edge. This is also consistent with the increase of butanol-infiltrated fiber loss at the wavelength greater than 1400 nm [55].

The temporal profile versus propagation length at various input pulse energies, and the pulse evolution of the SC along fiber #F₁ are described in Fig. 7 (b, c). OWB which induced by FWM begins at input pulse energy higher than 0.6 nJ, this can be observed at the blue-shifted (trailing) edge of the pulse and at the redshifted (leading) edge of the pulse. For the highest peak power 13.33 kW, the spectrum is asymmetric with respect to the pump wavelength and there is the tendency of spectral broadening towards the shorter wavelength due to the fact that the spectral broadening at the trailing edge of the pulse is inhibited by the low nonlinear coefficient and the high loss of butanol. SPM creates low frequencies at the front of the pulse, and high ones at the back. With the normal dispersion, group velocity dispersion lets low frequencies travel faster than high ones. In this case, the short wavelengths generated by SPM at the trailing edge propagate slower than the pulse tail at the pulse center. The interaction between these components leads to the onset of OWB at about 1050 nm with a propagation length of 4 cm of the fiber, and the new wavelengths can be created via four-wave mixing (FWM) [43, 45, 49].

The small dispersion value of -1.565 ps/nm.km at 1300 nm pump wavelength is also an essential factor contributing to the spectral extension of #F₁ fiber, a bandwidth of 714.37 nm is achieved with a maximum peak power of 13.33 kW. In work [32], the water-infiltrated SCF with all-normal dispersion can offer an SC spectrum of about 700 nm with a peak power of 20 kW which is about 1.5 times that of the #F₁ fiber. As for SCFs with air holes, 150 kW power (about 11 times more than #F₁ fibers) is required to generate SC with a broad spectrum of about 800 nm with all-normal dispersion [33].

#F₂ fiber has dispersion characteristics with both normal and anomalous regimes in the investigated wavelength range, two ZDWs are observed at 1.2887 μm (ZDW₁) and 1.439 μm (ZDW₂). In the simulation, we use the pump wavelengths at 1.3 μm which is located in an anomalous dispersion regime, near ZDW₁ with the pulse duration 120 ps. Figure 8 presents the numerical results of SC generation in #F₂ fiber. The spectral broadening is dominated by modulation instability, this makes the SC spectrum narrow when input energy is very low (0.05 nJ). With greater input energy, the

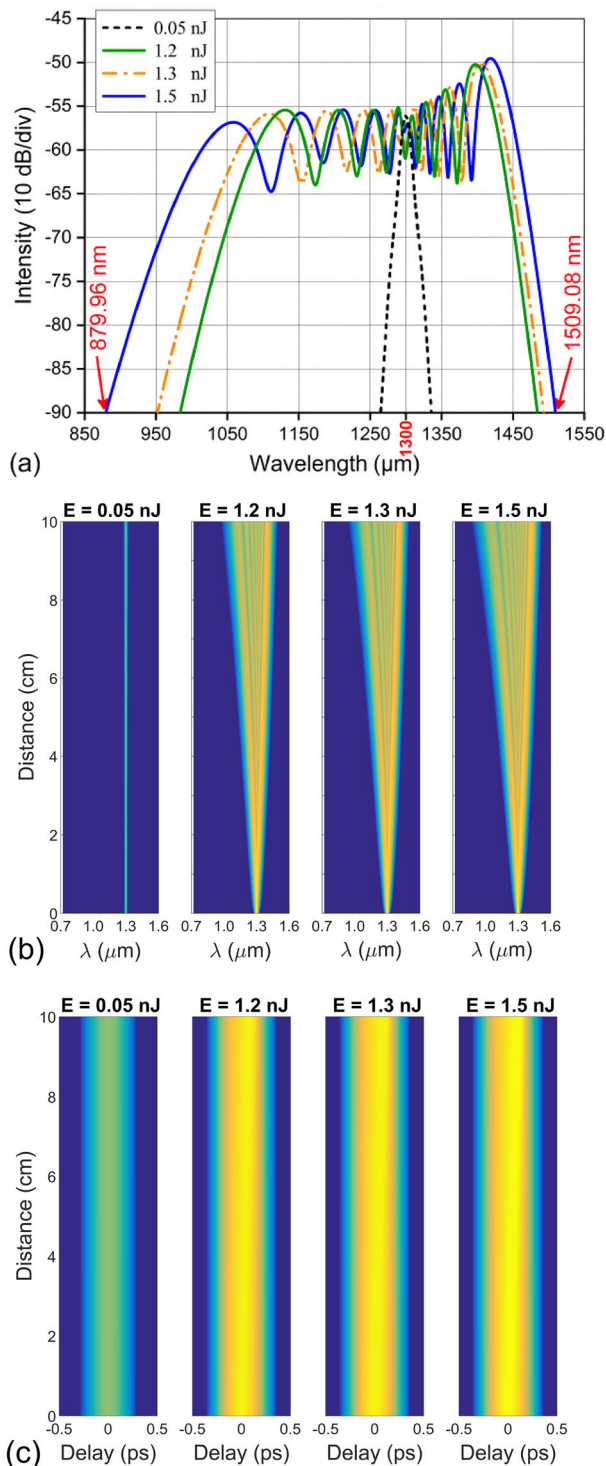


Fig. 8 For $\#F_2$ fiber: **a** various input pulse energy in 10 cm length when pumped with pulses of 120 ps duration, 1.3 μm pump wavelength, **b** the temporal profile versus propagation length at various input pulse energies, and **c** the pulse evolution of the SC along with fiber

SC spectrum is relatively flat and extended in an anomalous dispersion regime with 10 dB bandwidth. However, the difference between the spectral widths is not very large as the input energy continues to increase. For the case of 1.5 nJ input pulse energy (corresponding to a peak power of 12.5 kW), the SC spectrum expands from 0.72 to 0.2 μm (Fig. 8a).

With the selection of the pump wavelength in the anomalous dispersion mode, we expect the soliton dynamics with soliton fission to prevail in the spectral expansion. However, the supercontinuum results in Fig. 8 are observed to be in sharp contrast to standard photonic crystalline fibers with anomalous dispersion with only one zero dispersion wavelength or two widely separated zero dispersion wavelengths [56–59]. When the soliton fission is absent, the supercontinuum is expected to have less noise than the supercontinuum from conventional PCFs. In such fibers, the higher order-solitons evolve from the launched pulse. These solitons are unstable and split into fundamental solitons due to higher-order dispersion and Raman scattering while emitting blue-shifted non solitonic radiation. In this case, the SPM helps the spectrum to broaden and thus provides seed wavelengths for degenerate and non-degenerate four-wave mixing [56]. Soliton fission requires high intensity for phase matching when the excitation pulse propagates in PCFs with two widely separated ZDWs and FWM can be phase matched even with low intensity. This makes FWM a major cause for spectral expansion whereas the soliton dynamics are arrested and play an almost negligible role in the formation of the supercontinuum.

The evolution of the SC spectrum along the fiber and temporal profile at various propagation lengths in $\#F_2$ is shown in Fig. 8 (b, c). The SPM is the dominant nonlinear process here and the nonlinear dispersion properties are typical of those expected from their interaction in SCF. At the beginning of the propagation, the spectrum still has a shape characteristic of SPM. However, due to the high dispersion slope, the spectral broadening is limited in the short wavelength. During further propagation, FWM which is characterized by OWB, also contribute to the spectral extension at the wings but the low nonlinear coefficient is the main cause for limiting the spectral expansion in the long wavelength region. Due to the proximity of the pump wavelength (1.33 μm) and the ZDW₁ (1.2887 μm), a part of the spectrum is produced by SPM across the ZDW and experiences in normal-dispersion regime before soliton fission occurs. Unfortunately, soliton fission is not observed in anomalous SC generation for $\#F_2$ fiber as analyzed above. Mutual compensation of dispersion and SPM will not occur if the input energy is not large enough [56–58]. In Fig. 8a, the spectral width does not increase significantly in spite of the increased input energy which proves that 1.5 nJ achieved

is the largest input energy with femtosecond pulsed laser in performing these simulations.

Recently SG modeling results for silica-based PCF infiltrated with ethanol [39] were reported, the authors have shown that a PCF fiber of length 20 cm, with a pump wavelength of 1.55 μm , 50 kW peak power can generate 945 nm of flattened broadband SC. These results indicate a potential for further increased SC generation efficiency of our proposed butanol-suspended core fibers with approximately four times lower peak power. In addition, the obtained results indicated that all-normal and anomalous dispersion SC generation in proposed SCFs can be achieved at the same or even greater bandwidth with lower peak power than photonic crystal fibers infiltration with other liquids in previous works [32, 33, 38–40, 47].

Conclusion

For the first time, we have reported on supercontinuum generation in a PCF with a suspended core infiltrated with butanol. Both all-normal and anomalous dispersion are achieved by varying total diameter of the air-hole structure. Two optimal structures are proposed for use in SC generation with all-normal and anomalous dispersion properties. With the peak power of 13.33 kW, the broadening spectrum expanded from 806.19 nm to 1520.56 nm at 1.3 μm central wavelength for all-normal SC generation. In addition, for the anomalous SC generation, with two ZDWs close to each other, the spectrum is also extended from 879.96 nm to 1509.08 nm at 1.3 μm pump wavelength with the peak power of 12.5 kW. SPM at the center of the spectrum and OWB at the spectrum wings play a major role in spectral expansion for both cases. Soliton fission is not observed in anomalous SC generation.

The main reason for the moderate spectral width of the supercontinuum we have achieved is relatively low nonlinear coefficient and high loss of fibers. However, the suspended core structure and the infiltration of butanol into the air holes strongly influenced the dispersion of the fibers. The flat and small dispersion at the pump wavelength is completely beneficial for supercontinuum. In this case, the proposed fibers can offer reasonable, but not record-high broadening when they are pumped with low-energy sub-picosecond pulses. Considering the recent technological development of supercontinuum-based laser sources, we believe that the low input peak power and butanol infiltrated suspended core give both proposed fibers a high potential for a compact all-fiber SC generation system. Furthermore, this is a new class of fibers for all-fiber SC sources as an alternative to glass core fibers, since nonlinearity of butanol is higher than silica and its toxicity is negligible.

References

1. J.M. Dudley, G. Genty, S. Coen, *Rev. Mod. Phys.* (2006). <https://doi.org/10.1103/RevModPhys.78.1135>
2. S.D. Jackson, *Nat. Photon.* (2012). <https://doi.org/10.1038/nphoton.2012.149>
3. R.R. Alfano, *Sci. Am.* (2006) <https://www.jstor.org/stable/26069078>
4. K. Kosma, G. Zito, K. Schuster, S. Pissidakis, *Opt. Lett.* (2013). <https://doi.org/10.1364/OL.38.00130>
5. S.H. Kassani, R. Khazaeinezhad, Y. Jung, J. Kobelke, K. Oh, *IEEE Photon. J.* (2015). <https://doi.org/10.1109/JPHOT.2015.2396121>
6. N. Savage, *Nat. Photon.* (2009). <https://doi.org/10.1038/nphoton.2008.286>
7. J.T. Woodward, A.W. Smith, C.A. Jenkins, C. Lin, S.W. Brown, K.R. Lykke, *Metrologia* (2009). <https://doi.org/10.1088/0026-1394/46/4/S27>
8. F. Chu, G. Tsiminis, N.A. Spooner, T.M. Monro, *Sens. Act. B: Chem.* (2014). <https://doi.org/10.1016/j.snb.2014.03.031>
9. T.G. Euser, J.S.Y. Chen, M. Scharrer, P.J. Russell, N.J. Farrer, P.J. Sadler, *J. Appl. Phys.* (2008). <https://doi.org/10.1063/1.2924408>
10. C.R. Petersen, P.M. Moselund, L. Huot, L. Hooper, O. Bang, *Inf. Phys. Technol.* (2018). <https://doi.org/10.1016/j.infrared.2018.04.008>
11. A. Mazhorova, A. Markov, Ng. Andy, R. Chinnappan, O. Skorobogata, M. Zourob, M. Skorobogatiy, *Opt. Express* (2012). <https://doi.org/10.1364/OE.20.005344>
12. T.M. Monro, W. Belardi, K. Furusawa, J.C. Baggett, N.G.R. Broderick, D.J. Richardson, *Meas. Sci. Technol.* (2001). <https://doi.org/10.1088/0957-0233/12/7/318>
13. K.M. Kiang, K. Frampton, T.M. Monro, R. Moore, J. Tucknott, D.W. Hewak, D.J. Richardson, H.N. Rutt, *Electron. Lett.* (2002). <https://doi.org/10.1049/el:20020421>
14. V.V.R.K. Kumar, A.K. George, J.C. Knight, P.J. Russell, *Opt. Express* (2003). <https://doi.org/10.1364/OE.11.002641>
15. P. Petropoulos, H.E. Heidepriem, V. Finazzi, R.C. Moore, K. Frampton, D.J. Richardson, T.M. Monro, *Opt. Express* (2003). <https://doi.org/10.1364/OE.11.003568>
16. A.S. Webb, F. Poletti, D.J. Richardson, J.K. Sahu, *Opt. Eng.* (2007). <https://doi.org/10.1117/1.2430505>
17. L. Dong, B.K. Thomas, L. Fu, *Opt. Express* (2008). <https://doi.org/10.1364/OE.16.016423>
18. T.M. Monro, S.W. Smith, E.P. Schartner, A. François, A. Heng, H.E. Heidepriem, V.S. Afshar, *Opt. Fiber Technol.* (2010). <https://doi.org/10.1016/j.yofte.2010.09.010>
19. O. Frazão, R.M. Silva, M.S. Ferreira, J.L. Santos, A.B.L. Ribeiro, *Photon. Sens.* (2012). <https://doi.org/10.1007/s13320-012-0058-3>
20. H. Su, Y. Zhang, K. Ma, Y. Zhao, J. Wang, *Opt. Express.* (2019). <https://doi.org/10.1364/OE.27.020156>
21. C.M.B. Cordeiro, C.J.S. Matos, E.M. Santos, A. Bozolan, J.S.K. Ong, T. Facincani, G. Chesini, A.R. Vaz, C.H.B. Cruz, *Meas. Sci. Technol.* (2007). <https://doi.org/10.1088/0957-0233/18/10/S05>
22. W. Jiao, J. Liu, J. Zhang, G. Wang, M. Huan, *Appl. Sci.* (2018). <https://doi.org/10.3390/app8040592>
23. X. Zhang, X.S. Zhu, Y.W. Shi, *Opt. Lett.* (2019). <https://doi.org/10.1364/OL.44.004550>
24. C. Wang, W. Jin, C. Liao, J. Ma, W. Jin, F. Yang, H.L. Ho, Y. Wang, *Appl. Phys. Lett.* DOI **10**(1063/1), 4892962 (2014)
25. A.Y. Chamorovskiy, S.A. Nikitova, *J. Commun. Technol. Electron.* (2013). <https://doi.org/10.1134/S1064226913060053>
26. E. Coscelli, F. Poli, J. Li, A. Cutinotte, S. Selleri, *IEEE Photon. J.* (2015). <https://doi.org/10.1109/JPHOT.2015.2421436>
27. L. Fu, B.K. Thomas, L. Dong, *Opt. Express* (2008). <https://doi.org/10.1364/OE.16.019629>

28. I. Shavrin, S. Novotny, H. Ludvigsen, *Opt. Express* (2013). <https://doi.org/10.1364/OE.21.032141>
29. Y. Liu, Y. Zhao, J. Lyngsø, S. You, W.L. Wilson, H. Tu, S.A. Boppart, *J. Lightwave Technol.* (2015). <https://doi.org/10.1109/JLT.2015.2397276>
30. A.M. Heidt, A. Hartung, G.W. Bosman, P. Krok, E.G. Rohwer, H. Schwoerer, H. Bartelt, *Opt. Express* (2011). <https://doi.org/10.1364/OE.19.003775>
31. A. Hartung, A.M. Heidt, H. Bartelt, *Opt. Express* (2011). <https://doi.org/10.1364/OE.19.012275>
32. K.D. Xuan, L.C. Van, V.C. Long, Q.H. Dinh, L.V. Xuan, M. Trippenbach, R. Buczynski, *Appl. Opt.* (2017). <https://doi.org/10.1364/AO.56.001012>
33. T.L. Canh, V.T. Hoang, H.L. Van, D. Pysz, V.C. Long, T.B. Dinh, D.T. Nguyen, Q.H. Dinh, M. Klimczak, R. Kasztelanic, J. Pniewski, R. Buczynski, K.X. Dinh, *Opt. Mater. Express.* (2020). <https://doi.org/10.1364/OME.395936>
34. X. Zou, T. Izumitani, *J. Non-Cryst. Solids.* (1993). [https://doi.org/10.1016/0022-3093\(93\)90742-G](https://doi.org/10.1016/0022-3093(93)90742-G)
35. J.L. Vilas, J.A.S. Martin, E. Bernabeu, *Appl. Opt.* (2016). <https://doi.org/10.1364/AO.55.006222>
36. A. Sharafali, K. Nithyanandan, *Appl. Phys. B: Lasers Opt.* (2020). <https://doi.org/10.1007/s00340-020-7403-9>
37. T.N. Thi, D.H. Trong, B.T.L. Tran, T.D. Van, L.C. Van, *J. Opt.* (2022). <https://doi.org/10.1007/s12596-021-00802-y>
38. T.N. Thi, D.H. Trong, L.C. Van, *Laser Phys.* (2023). <https://doi.org/10.1088/1555-6611/acc240>
39. H.V. Le, V.L. Cao, H.T. Nguyen, A.M. Nguyen, R. Buczyński, R. Kasztelanic, *Laser Phys.* (2018). <https://doi.org/10.1088/1555-6611/aad93a>
40. L.C. Van, H.V. Le, N.D. Nguyen, N.V.T. Minh, Q.H. Dinh, V.T. Hoang, T.N. Thi, B.C. Van, *Laser Phys.* (2022). <https://doi.org/10.1088/1555-6611/ac599b>
41. L.C. Van, T.N. Thi, D.H. Trong, T.T.B. Le, N.V.T. Minh, V.T. Dang, T.L. Canh, D.Q. Ho, K.D. Quoc, *Opt. Quantum Electron.* (2022). <https://doi.org/10.1007/s11082-022-03667-y>
42. Z. Kang, F. Xu, J. Yuan, F. Li, B. Yan, X. Zhou, Q. Wu, K. Wang, X. Sang, K. Long, C. Yu, *IEEE J. Quantum Electron.* (2019). <https://doi.org/10.1109/JQE.2019.2901507>
43. T.N. Thi, D.H. Trong, L.C. Van, *Opt. Quantum Electron.* (2023). <https://doi.org/10.1007/s11082-022-04351-x>
44. L.C. Van, B.T.L. Tran, T.N. Thi, D.H. Trong, T.D. Van, T.D. Mai, H.T. Ngoc, T.T. Doan, K.D. Quoc, *Opt. Quantum Electron.* (2022). <https://doi.org/10.1007/s11082-022-04218-1>
45. T.N. Thi, D.H. Trong, B.T. Le Tran, L.C. Van, *J. Nonlinear Opt. Phys. Mater.* (2023). <https://doi.org/10.1142/S021886352350042X>
46. T.T.B. Le, O.T.T. Chuyen, T.N. Thi, L.C. Van, *Majlesi J. Electr. Eng.* (2022) <http://mjee.iaumajlesi.ac.ir/index/index.php/ee/article/view/4760>
47. V.T. Hoang, R. Kasztelanic, A. Filipkowski, G. Stępniewski, D. Pysz, M. Klimczak, S. Ertman, V.C. Long, T.R. Woliński, M. Trippenbach, K.D. Xuan, M. Śmietana, R. Buczyński, *Opt. Mater. Express* (2019). <https://doi.org/10.1364/OME.9.002264>
48. L.C. Van, A. Anuszkiewicz, A. Ramaniuk, R. Kasztelanic, K.D. Xuan, V.C. Long, M. Trippenbach, R. Buczyński, *J. Opt.* (2017). <https://doi.org/10.1088/2040-8986/aa96bc>
49. A. Sharafali, A.K. Shafeeque Ali, M. Lakshmanan, *Phys Lett A* (2021). <https://doi.org/10.1016/j.physleta.2021.127290>
50. K. Moutzouris, M. Papamichael, S.C. Betsis, I. Stavrakas, G. Hloupis, D. Triantis, *Appl. Phys. B.* (2014). <https://doi.org/10.1007/s00340-013-5744-3>
51. I.H. Malitson, *Opt. Soc. Am.* (1965). <https://doi.org/10.1364/JOSA.55.001205>
52. J.M. Dudley, J.R. Taylor, *Supercontinuum generation in optical fibers*, 1st edn. (Cambridge University Press, Cambridge, 2010). <https://doi.org/10.1017/CBO9780511750465>
53. C. Finot, B. Kibler, L. Provost, S. Wabnitz, *J. Opt. Soc. Am. B.* (2008). <https://doi.org/10.1364/JOSAB.25.001938>
54. L.C. Van, T.N. Thi, B.T.L. Tran, D.H. Trong, N.V.T. Minh, H.V. Le, V.T. Hoang, *Photon. Nanostruct. Fundam. Applic.* (2022). <https://doi.org/10.1016/j.photonics.2021.100986>
55. J. Park, D.E. Kang, B. Paulson, T. Nazari, K. Oh, *Opt. Express.* (2014). <https://doi.org/10.1364/OE.22.017320>
56. A.M. Heidt, *J. Opt. Soc. Am. B.* (2010). <https://doi.org/10.1364/JOSAB.27.000550>
57. A. Ghanbari, A. Kashaninia, A. Sadr, H. Saghaei, *Optik* (2017). <https://doi.org/10.1016/j.ijleo.2017.04.099>
58. L. Tian, L. Wei, F. Guoying, *Opt. Commun.* (2015). <https://doi.org/10.1016/j.optcom.2014.07.080>
59. K.M. Hilligsøe, T.V. Andersen, H.N. Paulsen, C.K. Nielsen, K. Mølmer, S. Keiding, R. Kristiansen, K.P. Hansen, J.J. Larsen, *Opt. Express* (2004). <https://doi.org/10.1364/OPEX.12.001045>

Publisher's Note Springer Nature remains neutral with regard to jurisdictional claims in published maps and institutional affiliations.

Springer Nature or its licensor (e.g. a society or other partner) holds exclusive rights to this article under a publishing agreement with the author(s) or other rightsholder(s); author self-archiving of the accepted manuscript version of this article is solely governed by the terms of such publishing agreement and applicable law.